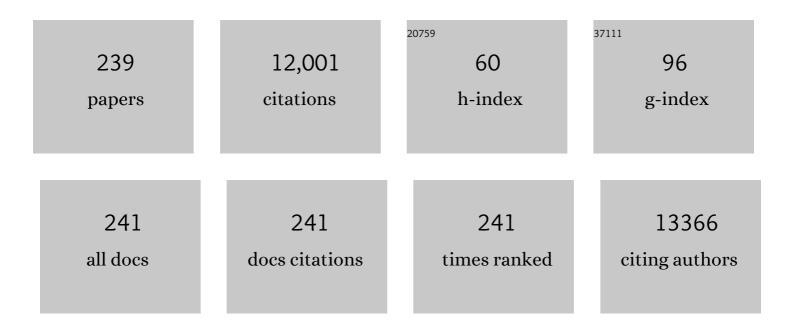
Qingzhong Xue

List of Publications by Year in descending order

Source: https://exaly.com/author-pdf/3771488/publications.pdf Version: 2024-02-01



#	Article	IF	CITATIONS
1	Fabrication and characterization of an ultrasensitive humidity sensor based on metal oxide/graphene hybrid nanocomposite. Sensors and Actuators B: Chemical, 2016, 225, 233-240.	4.0	367
2	Layered double hydroxides toward high-performance supercapacitors. Journal of Materials Chemistry A, 2017, 5, 15460-15485.	5.2	326
3	Graphene oxide/polyacrylonitrile fiber hierarchical-structured membrane for ultra-fast microfiltration of oil-water emulsion. Chemical Engineering Journal, 2017, 307, 643-649.	6.6	303
4	Flexible self-powered high-performance ammonia sensor based on Au-decorated MoSe2 nanoflowers driven by single layer MoS2-flake piezoelectric nanogenerator. Nano Energy, 2019, 65, 103974.	8.2	281
5	Ultrahigh performance humidity sensor based on layer-by-layer self-assembly of graphene oxide/polyelectrolyte nanocomposite film. Sensors and Actuators B: Chemical, 2014, 203, 263-270.	4.0	242
6	Stable CoSe ₂ /carbon nanodice@reduced graphene oxide composites for high-performance rechargeable aluminum-ion batteries. Energy and Environmental Science, 2018, 11, 2341-2347.	15.6	240
7	Critical role of small micropores in high CO2 uptake. Physical Chemistry Chemical Physics, 2013, 15, 2523.	1.3	228
8	Influence of chemical functionalization on the CO2/N2 separation performance of porous graphene membranes. Nanoscale, 2012, 4, 5477.	2.8	193
9	Investigation of Molecular Interactions between SWNT and Polyethylene/Polypropylene/Polystyrene/Polyaniline Molecules. Journal of Physical Chemistry C, 2007, 111, 4628-4635.	1.5	176
10	Iron-doping-enhanced photoelectrochemical water splitting performance of nanostructured WO ₃ : a combined experimental and theoretical study. Nanoscale, 2015, 7, 2933-2940.	2.8	171
11	Antifouling hydrolyzed polyacrylonitrile/graphene oxide membrane with spindle-knotted structure for highly effective separation of oil-water emulsion. Journal of Membrane Science, 2017, 532, 38-46.	4.1	170
12	Understanding the relationship between ion migration and the anomalous hysteresis in high-efficiency perovskite solar cells: A fresh perspective from halide substitution. Nano Energy, 2016, 26, 620-630.	8.2	167
13	Superior capacitive performance of active carbons derived from Enteromorpha prolifera. Electrochimica Acta, 2014, 133, 459-466.	2.6	162
14	Tunable Hydrogen Separation in Porous Graphene Membrane: First-Principle and Molecular Dynamic Simulation. ACS Applied Materials & Interfaces, 2014, 6, 8048-8058.	4.0	159
15	C ₂ N: an excellent two-dimensional monolayer membrane for He separation. Journal of Materials Chemistry A, 2015, 3, 21351-21356.	5.2	157
16	Model for the effective thermal conductivity of carbon nanotube composites. Nanotechnology, 2006, 17, 1655-1660.	1.3	155
17	Effect of Chemisorption on the Interfacial Bonding Characteristics of Grapheneâ^'Polymer Composites. Journal of Physical Chemistry C, 2010, 114, 6588-6594.	1.5	150
18	High-rate capacitive performance of graphene aerogel with a superhigh C/O molar ratio. Journal of Materials Chemistry, 2012, 22, 23186.	6.7	145

#	Article	IF	CITATIONS
19	Effect of defects on Young's modulus of graphene sheets: a molecular dynamics simulation. RSC Advances, 2012, 2, 9124.	1.7	142
20	Ultra-sensitive NH3 sensor based on flower-shaped SnS2 nanostructures with sub-ppm detection ability. Journal of Hazardous Materials, 2018, 341, 159-167.	6.5	140
21	Electrical and photovoltaic characteristics of MoS2/Si <i>p-n</i> junctions. Journal of Applied Physics, 2015, 117, .	1.1	131
22	The influence of particle shape and size on electric conductivity of metal–polymer composites. European Polymer Journal, 2004, 40, 323-327.	2.6	129
23	Computational analysis of effect of modification on the interfacial characteristics of a carbon nanotube–polyethylene composite system. Applied Surface Science, 2009, 255, 3534-3543.	3.1	127
24	Fabrication of Carbon Nanoscrolls from Monolayer Graphene. Small, 2010, 6, 2010-2019.	5.2	127
25	Theoretical approaches to graphene and graphene-based materials. Nano Today, 2012, 7, 180-200.	6.2	122
26	A hierarchical structured steel mesh decorated with metal organic framework/graphene oxide for high-efficient oil/water separation. Journal of Hazardous Materials, 2019, 373, 725-732.	6.5	120
27	Fluorine-Modified Porous Graphene as Membrane for CO ₂ /N ₂ Separation: Molecular Dynamic and First-Principles Simulations. Journal of Physical Chemistry C, 2014, 118, 7369-7376.	1.5	114
28	Charge-modulated CO2 capture of C3N nanosheet: Insights from DFT calculations. Chemical Engineering Journal, 2018, 338, 92-98.	6.6	111
29	ZIF-derived porous ZnO-Co3O4 hollow polyhedrons heterostructure with highly enhanced ethanol detection performance. Sensors and Actuators B: Chemical, 2017, 253, 523-532.	4.0	108
30	Pore-scale characterization of tight sandstone in Yanchang Formation Ordos Basin China using micro-CT and SEM imaging from nm- to cm-scale. Fuel, 2017, 209, 254-264.	3.4	107
31	Electrostatic Self-Assembly of Sandwich-Like CoAl-LDH/Polypyrrole/Graphene Nanocomposites with Enhanced Capacitive Performance. ACS Applied Materials & amp; Interfaces, 2017, 9, 31699-31709.	4.0	103
32	High-efficiency separation performance of oil-water emulsions of polyacrylonitrile nanofibrous membrane decorated with metal-organic frameworks. Applied Surface Science, 2019, 476, 61-69.	3.1	103
33	Adsorption and Catalytic Activation of O ₂ Molecule on the Surface of Au-Doped Graphene under an External Electric Field. Journal of Physical Chemistry C, 2012, 116, 19918-19924.	1.5	99
34	High-performance n-MoS ₂ /i-SiO ₂ /p-Si heterojunction solar cells. Nanoscale, 2015, 7, 8304-8308.	2.8	99
35	Effect of chemisorption on the interfacial bonding characteristics of carbon nanotube–polymer composites. Polymer, 2008, 49, 800-808.	1.8	96
36	Synthesis of nanowire bundle-like WO3-W18O49 heterostructures for highly sensitive NH3 sensor application. Journal of Hazardous Materials, 2018, 353, 290-299.	6.5	94

#	Article	IF	CITATIONS
37	Carbon-encapsulated CoSe nanoparticles derived from metal-organic frameworks as advanced cathode material for Al-ion battery. Journal of Power Sources, 2018, 401, 6-12.	4.0	94
38	Dual-functional membrane decorated with flower-like metal–organic frameworks for highly efficient removal of insoluble emulsified oils and soluble dyes. Journal of Hazardous Materials, 2021, 408, 124444.	6.5	92
39	The interface effect of the effective electrical conductivity of carbon nanotube composites. Nanotechnology, 2007, 18, 255705.	1.3	89
40	Reusable membrane with multifunctional skin layer for effective removal of insoluble emulsified oils and soluble dyes. Journal of Hazardous Materials, 2021, 415, 125677.	6.5	86
41	Temperature dependence of the electrical properties of the carbon nanotube/polymer composites. EXPRESS Polymer Letters, 2009, 3, 769-777.	1.1	85
42	Keys to linking GCMC simulations and shale gas adsorption experiments. Fuel, 2017, 199, 14-21.	3.4	84
43	Large dielectric constant of the chemically purified carbon nanotube/polymer composites. Materials Letters, 2008, 62, 4229-4231.	1.3	82
44	Porous graphene sandwich/poly(vinylidene fluoride) composites with high dielectric properties. Composites Science and Technology, 2013, 86, 70-75.	3.8	79
45	Superior Selective CO ₂ Adsorption of C ₃ N Pores: GCMC and DFT Simulations. ACS Applied Materials & Interfaces, 2017, 9, 31161-31169.	4.0	79
46	The Core/Shell Composite Nanowires Produced by Self-Scrolling Carbon Nanotubes onto Copper Nanowires. ACS Nano, 2009, 3, 2235-2240.	7.3	78
47	Gigantic enhancement in the dielectric properties of polymer-based composites using core/shell MWCNT/amorphous carbon nanohybrids. Nanoscale, 2015, 7, 3660-3667.	2.8	78
48	Multi-shelled ZnCo2O4 yolk-shell spheres for high-performance acetone gas sensor. Applied Surface Science, 2018, 443, 114-121.	3.1	77
49	UV assisted ppb-level acetone detection based on hollow ZnO/MoS2 nanosheets core/shell heterostructures at low temperature. Sensors and Actuators B: Chemical, 2020, 317, 128208.	4.0	74
50	Chemically functionalized 3D reticular graphene oxide frameworks decorated with MOF-derived Co3O4: Towards highly sensitive and selective detection to acetone. Sensors and Actuators B: Chemical, 2018, 259, 289-298.	4.0	73
51	Flexible SnSe Photodetectors with Ultrabroad Spectral Response up to 10.6 μm Enabled by Photobolometric Effect. ACS Applied Materials & Interfaces, 2020, 12, 35250-35258.	4.0	73
52	SnO2 nanoparticles-modified 3D-multilayer MoS2 nanosheets for ammonia gas sensing at room temperature. Sensors and Actuators B: Chemical, 2020, 321, 128471.	4.0	71
53	Effective CO2 detection based on LaOCl-doped SnO2 nanofibers: Insight into the role of oxygen in carrier gas. Sensors and Actuators B: Chemical, 2017, 241, 725-734.	4.0	69
54	Superhigh-rate capacitive performance of heteroatoms-doped double shell hollow carbon spheres. Carbon, 2015, 86, 235-244.	5.4	68

#	Article	IF	CITATIONS
55	Insight of synergistic effect of different active metal ions in layered double hydroxides on their electrochemical behaviors. Electrochimica Acta, 2017, 253, 302-310.	2.6	67
56	On the origin of the high capacitance of carbon derived from seaweed with an apparently low surface area. Journal of Materials Chemistry A, 2014, 2, 18998-19004.	5.2	65
57	Theoretical study of a tunable and strain-controlled nanoporous graphenylene membrane for multifunctional gas separation. Journal of Materials Chemistry A, 2016, 4, 15015-15021.	5.2	65
58	Great enhancement of CH4 sensitivity of SnO2 based nanofibers by heterogeneous sensitization and catalytic effect. Sensors and Actuators B: Chemical, 2018, 254, 393-401.	4.0	65
59	Sandwich-like graphene/polypyrrole/layered double hydroxide nanowires for high-performance supercapacitors. Journal of Power Sources, 2016, 331, 67-75.	4.0	62
60	Co-MOF-74 derived Co3O4/graphene heterojunction nanoscrolls for ppb-level acetone detection. Sensors and Actuators B: Chemical, 2019, 300, 127011.	4.0	62
61	Enhancing oil-in-water emulsion separation performance of polyvinyl alcohol hydrogel nanofibrous membrane by squeezing coalescence demulsification. Journal of Membrane Science, 2021, 630, 119324.	4.1	61
62	Room-temperature high-sensitivity detection of ammonia gas using the capacitance of carbon/silicon heterojunctions. Energy and Environmental Science, 2010, 3, 288.	15.6	60
63	Pinning Down the Anomalous Light Soaking Effect toward High-Performance and Fast-Response Perovskite Solar Cells: The Ion-Migration-Induced Charge Accumulation. Journal of Physical Chemistry Letters, 2017, 8, 5069-5076.	2.1	60
64	Glass transition temperature of functionalized graphene–polymer composites. Computational Materials Science, 2013, 71, 66-71.	1.4	58
65	Extraction of kerogen from oil shale with supercritical carbon dioxide: Molecular dynamics simulations. Journal of Supercritical Fluids, 2016, 107, 499-506.	1.6	58
66	Self-powered multifunctional monitoring and analysis system based on dual-triboelectric nanogenerator and chitosan/activated carbon film humidity sensor. Nano Energy, 2022, 94, 106881.	8.2	58
67	Metal-organic frameworks derived ZnO@MoS nanosheets core/shell heterojunctions for ppb-level acetone detection: Ultra-fast response and recovery. Sensors and Actuators B: Chemical, 2020, 304, 127430.	4.0	57
68	Insight into high areal capacitances of low apparent surface area carbons derived from nitrogen-rich polymers. Carbon, 2015, 94, 560-567.	5.4	56
69	Waterâ€5oluble Salt Templateâ€Assisted Anchor of Hollow FeS ₂ Nanoparticle Inside 3D Carbon Skeleton to Achieve Fast Potassiumâ€ion Storage. Advanced Energy Materials, 2021, 11, 2101343.	10.2	56
70	GCMC simulations on the adsorption mechanisms of CH4 and CO2 in K-illite and their implications for shale gas exploration and development. Fuel, 2018, 224, 521-528.	3.4	55
71	Sandwich-like nitrogen-doped porous carbon/graphene nanoflakes with high-rate capacitive performance. Nanoscale, 2016, 8, 7889-7898.	2.8	54
72	Effects of Sulfur Doping and Humidity on CO ₂ Capture by Graphite Split Pore: A Theoretical Study. ACS Applied Materials & Interfaces, 2017, 9, 8336-8343.	4.0	53

#	Article	IF	CITATIONS
73	Remarkable supercapacitor performance of petal-like LDHs vertically grown on graphene/polypyrrole nanoflakes. Journal of Materials Chemistry A, 2017, 5, 8964-8971.	5.2	53
74	Wafer-size growth of 2D layered SnSe films for UV-Visible-NIR photodetector arrays with high responsitivity. Nanoscale, 2020, 12, 7358-7365.	2.8	53
75	Metal-organic frameworks derived hierarchical flower-like ZnO/ Co3O4 heterojunctions for ppb-level acetone detection. Sensors and Actuators B: Chemical, 2020, 325, 128814.	4.0	52
76	Inherent wettability of different rock surfaces at nanoscale: a theoretical study. Applied Surface Science, 2018, 434, 73-81.	3.1	51
77	A durable mesh decorated with polydopamine/graphene oxide for highly efficient oil/water mixture separation. Applied Surface Science, 2019, 479, 351-359.	3.1	51
78	Enhanced gas separation performance of Pebax mixed matrix membranes by incorporating ZIF-8 in situ inserted by multiwalled carbon nanotubes. Separation and Purification Technology, 2020, 248, 117080.	3.9	49
79	Molecular insights into carbon dioxide enhanced multi-component shale gas recovery and its sequestration in realistic kerogen. Chemical Engineering Journal, 2021, 425, 130292.	6.6	49
80	Excellent dielectric properties of Polyvinylidene fluoride composites based on sandwich structured MnO2/graphene nanosheets/MnO2. Composites Part A: Applied Science and Manufacturing, 2014, 67, 252-258.	3.8	47
81	Graphitic carbon nitride catalyzes selective oxidative dehydrogenation of propane. Applied Catalysis B: Environmental, 2020, 262, 118277.	10.8	47
82	Effect of chemisorption structure on the interfacial bonding characteristics of graphene–polymer composites. Applied Surface Science, 2012, 258, 2077-2082.	3.1	46
83	Electrical characterization and ammonia sensing properties of MoS2/Si p–n junction. Journal of Alloys and Compounds, 2015, 631, 105-110.	2.8	46
84	ZIF-8 derived ZnO polyhedrons decorated with biomass derived nitrogen-doped porous carbon for enhanced acetone sensing. Sensors and Actuators B: Chemical, 2021, 330, 129366.	4.0	46
85	Influence of Nanotube Chirality, Temperature, and Chemical Modification on the Interfacial Bonding between Carbon Nanotubes and Polyphenylacetylene. Journal of Physical Chemistry C, 2008, 112, 16514-16520.	1.5	45
86	Investigation of pore size effects on adsorption behavior of shale gas. Marine and Petroleum Geology, 2019, 109, 1-8.	1.5	45
87	Multifunctional charged hydrogel nanofibrous membranes for metal ions contained emulsified oily wastewater purification. Journal of Membrane Science, 2021, 621, 118950.	4.1	45
88	Self-powered broadband, high-detectivity and ultrafast photodetectors based on Pd-MoS ₂ /Si heterojunctions. Physical Chemistry Chemical Physics, 2016, 18, 1131-1139.	1.3	44
89	Enhanced Room Temperature Oxygen Sensing Properties of LaOCl–SnO ₂ Hollow Spheres by UV Light Illumination. ACS Sensors, 2017, 2, 679-686.	4.0	43
90	Carbon Doping of Hexagonal Boron Nitride by Using CO Molecules. Journal of Physical Chemistry C, 2013, 117, 9332-9339.	1.5	42

#	Article	IF	CITATIONS
91	How to select an optimal surfactant molecule to speed up the oil-detachment from solid surface: A computational simulation. Chemical Engineering Science, 2016, 147, 47-53.	1.9	42
92	Ultrahigh broadband photoresponse of SnO ₂ nanoparticle thin film/SiO ₂ /p-Si heterojunction. Nanoscale, 2017, 9, 8848-8857.	2.8	41
93	Enhanced energy storage density and discharge efficiency in potassium sodium niobite-based ceramics prepared using a new scheme. Journal of the European Ceramic Society, 2020, 40, 2357-2365.	2.8	41
94	Self-assembly of double helical nanostructures inside carbon nanotubes. Nanoscale, 2013, 5, 4191.	2.8	40
95	Effective enhancement of gas separation performance in mixed matrix membranes using core/shell structured multi-walled carbon nanotube/graphene oxide nanoribbons. Nanotechnology, 2017, 28, 065702.	1.3	40
96	Bioinspired Anti-Oil-Fouling Hierarchical Structured Membranes Decorated with Urchin-Like α-FeOOH Particles for Efficient Oil/Water Mixture and Crude Oil-in-Water Emulsion Separation. ACS Applied Materials & Interfaces, 2020, 12, 50962-50970.	4.0	40
97	Room temperature hydrogen sensor with ultrahigh-responsive characteristics based on Pd/SnO2/SiO2/Si heterojunctions. Sensors and Actuators B: Chemical, 2016, 227, 438-447.	4.0	39
98	Fabrication of Carbon Nanoscrolls from Monolayer Graphene Controlled by P-Doped Silicon Nanowires: A MD Simulation Study. Journal of Physical Chemistry C, 2011, 115, 15217-15224.	1.5	37
99	Outstanding capacitive performance of ordered mesoporous carbon modified by anthraquinone. Electrochimica Acta, 2018, 259, 110-121.	2.6	37
100	Polycyclic Aromatic Hydrocarbons as a New Class of Promising Cathode Materials for Aluminumâ€lon Batteries. Angewandte Chemie - International Edition, 2022, 61, e202114681.	7.2	37
101	Structure control of ultra-large graphene oxide sheets by the Langmuir–Blodgett method. RSC Advances, 2013, 3, 4680.	1.7	36
102	Theoretical Prediction of Hydrogen Separation Performance of Two-Dimensional Carbon Network of Fused Pentagon. ACS Applied Materials & Interfaces, 2015, 7, 28502-28507.	4.0	36
103	Oil detachment from silica surface modified by carboxy groups in aqueous cetyltriethylammonium bromide solution. Applied Surface Science, 2015, 353, 1103-1111.	3.1	36
104	High hydrogen sensitivity of vertically standing layered MoS2/Si heterojunctions. Journal of Alloys and Compounds, 2016, 682, 29-34.	2.8	36
105	Facile synthesis of La 2 O 2 CO 3 nanoparticle films and Its CO 2 sensing properties and mechanisms. Applied Surface Science, 2017, 426, 725-733.	3.1	36
106	3D radial Co3O4 nanorod cluster derived from cobalt-based layered hydroxide metal salt for enhanced trace acetone detection. Sensors and Actuators B: Chemical, 2021, 327, 128926.	4.0	36
107	Ammonia sensitivity of amorphous carbon film/silicon heterojunctions. Applied Physics Letters, 2007, 91, .	1.5	35
108	High-performance WO _{3â^'x} -WSe ₂ /SiO ₂ /n-Si heterojunction near-infrared photodetector <i>via</i> a homo-doping strategy. Journal of Materials Chemistry C, 2018, 6, 5821-5829.	2.7	34

#	Article	IF	CITATIONS
109	Hydrogen storage and release by bending carbon nanotubes. Computational Materials Science, 2013, 68, 121-126.	1.4	33
110	585 divacancy-defective germanene as a hydrogen separation membrane: A DFT study. International Journal of Hydrogen Energy, 2017, 42, 24189-24196.	3.8	33
111	High performance aluminum ion battery using polyaniline/ordered mesoporous carbon composite. Journal of Power Sources, 2020, 477, 228702.	4.0	33
112	Current–voltage characteristics and ethanol gas sensing properties of ZnO thin film/Si heterojunction at room temperature. Physica E: Low-Dimensional Systems and Nanostructures, 2010, 42, 2021-2025.	1.3	32
113	Outstanding capacitive performance of reticular porous carbon/graphene sheets with superhigh surface area. Electrochimica Acta, 2016, 190, 923-931.	2.6	32
114	Stimulation of surface terminating group by carbon quantum dots for improving pseudocapacitance of Ti3C2Tx MXene based electrode. Carbon, 2021, 180, 118-126.	5.4	32
115	Highly enhanced sensitivity of hydrogen sensors using novel palladium-decorated graphene nanoribbon film/SiO ₂ /Si structures. Journal of Materials Chemistry A, 2014, 2, 15931-15937.	5.2	31
116	β-Hydrogen of Polythiophene Induced Aluminum Ion Storage for High-Performance Al-Polythiophene Batteries. ACS Applied Materials & Interfaces, 2020, 12, 46065-46072.	4.0	31
117	High-performance aluminum-polyaniline battery based on the interaction between aluminum ion and -NH groups. Science China Materials, 2021, 64, 318-328.	3.5	31
118	Radial Collapse of Single-Walled Carbon Nanotubes Induced by the Cu ₂ O Surface. Journal of Physical Chemistry C, 2009, 113, 3120-3126.	1.5	30
119	Ultrafast breathing humidity sensing properties of low-dimensional Fe-doped SnO ₂ flower-like spheres. RSC Advances, 2016, 6, 27008-27015.	1.7	30
120	Bifuntional petaloid nickel manganese layered double hydroxides decorated on a freestanding carbon foam for flexible asymmetric supercapacitor and oxygen evolution. Electrochimica Acta, 2017, 252, 275-285.	2.6	30
121	Influence of Solid Surface and Functional Group on the Collapse of Carbon Nanotubes. Journal of Physical Chemistry C, 2010, 114, 2100-2107.	1.5	28
122	Effect of ethanol gas on the electrical properties of ZnO nanorods. Physica E: Low-Dimensional Systems and Nanostructures, 2011, 43, 1056-1060.	1.3	28
123	Mechanism of oil molecules transportation in nano-sized shale channel: MD simulation. RSC Advances, 2015, 5, 25684-25692.	1.7	28
124	Two-dimensional graphene oxide membrane for H2/CH4 separation: Insights from molecular dynamics simulations. International Journal of Hydrogen Energy, 2017, 42, 30653-30660.	3.8	28
125	Revealing the impacting factors of cathodic carbon catalysts for Li-CO2 batteries in the pore-structure point of view. Electrochimica Acta, 2019, 311, 41-49.	2.6	28
126	One-step synthesis of a robust and anti-oil-fouling biomimetic cactus-like hierarchical architecture for highly efficient oil/water separation. Environmental Science: Nano, 2020, 7, 903-911.	2.2	28

#	Article	IF	CITATIONS
127	Self-assembly of C4H-type hydrogenated graphene. Nanoscale, 2013, 5, 11132.	2.8	27
128	Hydrogen gas sensing properties of Pd/a-C:Pd/SiO2/Si structure at room temperature. Sensors and Actuators B: Chemical, 2013, 186, 796-801.	4.0	27
129	Growth and humidity-dependent electrical properties of bulk-like MoS ₂ thin films on Si. RSC Advances, 2015, 5, 74329-74335.	1.7	27
130	Me–N–C (Me = Fe, Cu, and Co) nanosheet as a promising charge-controlled CO2 capture material. Journal of Materials Chemistry A, 2018, 6, 12404-12410.	5.2	27
131	Charge-controlled switchable H2 storage on conductive borophene nanosheet. International Journal of Hydrogen Energy, 2019, 44, 20150-20157.	3.8	26
132	Oxygen vacancies enhanced photoresponsive performance of ZnO nanoparticles thin film/Si heterojunctions for ultraviolet/infrared photodetector. Journal of Alloys and Compounds, 2019, 797, 1224-1231.	2.8	26
133	Layered double hydroxides derived NiCo-sulfide as a cathode material for aluminum ion batteries. Electrochimica Acta, 2020, 344, 136174.	2.6	26
134	Bimetallic metal–organic frameworks derived hierarchical flower-like Zn-doped Co3O4 for enhanced acetone sensing properties. Applied Surface Science, 2021, 565, 150520.	3.1	26
135	The miscible behaviors and mechanism of CO2/CH4/C3H8/N2 and crude oil in nanoslits: A molecular dynamics simulation study. Fuel, 2021, 304, 121461.	3.4	26
136	Humidity sensitive properties of amorphous (K,Na)NbO3 lead free thin films. Ceramics International, 2014, 40, 10263-10267.	2.3	25
137	High hydrogen response of Pd/TiO2/SiO2/Si multilayers at room temperature. Sensors and Actuators B: Chemical, 2014, 205, 255-260.	4.0	25
138	Excellent dielectric properties of PVDF-based composites filled with carbonized PAN/PEG copolymer fibers. Composites Part A: Applied Science and Manufacturing, 2016, 87, 46-53.	3.8	25
139	Dynamics and miscible behaviors of hydrocarbon gas and crude oil in nanoslits: Effects of light gas type and crude oil components. Chemical Engineering Journal, 2021, 405, 127012.	6.6	25
140	Anomalous positive magnetoresistance in Cox–C1â^'x granular films on Si substrates. Journal of Applied Physics, 2004, 95, 1906-1910.	1.1	24
141	Small graphite nanoflakes as an advanced cathode material for aluminum ion batteries. Chemical Communications, 2020, 56, 1593-1596.	2.2	24
142	Microphone-like Cu-CAT-1 hierarchical structures with ultra-low oil adhesion for highly efficient oil/water separation. Separation and Purification Technology, 2020, 241, 116688.	3.9	24
143	Critical factors controlling adsorption capacity of shale gas in Wufeng-Longmaxi formation, Sichuan Basin: Evidences from both experiments and molecular simulations. Journal of Natural Gas Science and Engineering, 2021, 88, 103774.	2.1	24
144	Hierarchical superhydrophobic polydimethylsiloxane/copper terephthalate/polyurethane sponge for highly efficient oil/water separation. Colloids and Surfaces A: Physicochemical and Engineering Aspects, 2021, 630, 127635.	2.3	24

#	Article	IF	CITATIONS
145	Sulfur–Nitrogen Codoped Graphite Slit-Pore for Enhancing Selective Carbon Dioxide Adsorption: Insights from Molecular Simulations. ACS Sustainable Chemistry and Engineering, 2017, 5, 8815-8823.	3.2	23
146	Adsorption and absorption of supercritical methane within shale kerogen slit. Journal of Molecular Liquids, 2020, 320, 114364.	2.3	23
147	Different factors' effect on the SWNT-fluorocarbon resin interaction: A MD simulation study. Computational Materials Science, 2010, 49, 148-157.	1.4	22
148	Silicon/graphene core/shell nanowires produced by self-scrolling. Computational Materials Science, 2010, 49, 588-592.	1.4	22
149	Ultra-high selective capture of CO 2 on one-sided N-doped carbon nanoscrolls. Journal of CO2 Utilization, 2017, 18, 275-282.	3.3	22
150	Critical factors controlling shale gas adsorption mechanisms on Different Minerals Investigated Using GCMC simulations. Marine and Petroleum Geology, 2019, 100, 31-42.	1.5	22
151	Embedded SnO2/Diatomaceous earth composites for fast humidity sensing and controlling properties. Sensors and Actuators B: Chemical, 2020, 303, 127137.	4.0	22
152	Super flexibility and stability of graphene nanoribbons under severe twist. Physical Chemistry Chemical Physics, 2016, 18, 18406-18413.	1.3	21
153	Preparation of spherical and dendritic CdS@TiO2 hollow double-shelled nanoparticles for photocatalysis. Materials Letters, 2016, 166, 113-115.	1.3	21
154	Ultrahigh photosensitivity and detectivity of hydrogen-treated TiO ₂ nanorod array/SiO ₂ /Si heterojunction broadband photodetectors and its mechanism. Journal of Materials Chemistry C, 2018, 6, 2319-2328.	2.7	21
155	Doping-induced enhancement of CO2 adsorption on negatively charged C3N nanosheet: Insights from DFT calculations. Chemical Engineering Journal, 2020, 387, 123403.	6.6	21
156	A percolation model of metal–insulator composites. Physica B: Condensed Matter, 2003, 325, 195-198.	1.3	20
157	Chemical Modification: an Effective Way of Avoiding the Collapse of SWNTs on Al Surface Revealed by Molecular Dynamics Simulations. Journal of Physical Chemistry C, 2009, 113, 14747-14752.	1.5	20
158	Diverse nanowires activated self-scrolling of graphene nanoribbons. Applied Surface Science, 2012, 258, 1964-1970.	3.1	20
159	Release of encapsulated molecules from carbon nanotubes using a displacing method: a MD simulation study. RSC Advances, 2012, 2, 6913.	1.7	20
160	Self-Assembly of Helical Polyacetylene Nanostructures on Carbon Nanotubes. Journal of Physical Chemistry C, 2013, 117, 16248-16255.	1.5	20
161	The preparation, load and photocatalytic performance of N-doped and CdS-coupled TiO2. RSC Advances, 2013, 3, 9483.	1.7	20
162	Solution quenched in-situ growth of hierarchical flower-like NiFe2O4/Fe2O3 heterojunction for wide-range light absorption. Journal of Power Sources, 2019, 440, 227120.	4.0	20

#	Article	IF	CITATIONS
163	Layer-by-layer self-assembly of polyaniline nanofibers/TiO ₂ nanotubes heterojunction thin film for ammonia detection at room temperature. Nanotechnology, 2019, 30, 135501.	1.3	20
164	Effective dielectric constant of composite with interfacial shells. Physica B: Condensed Matter, 2004, 344, 129-132.	1.3	19
165	The miscible behaviors of C10H22(C7H17N)/C3H8 system: Insights from molecular dynamics simulations. Fuel, 2020, 279, 118445.	3.4	19
166	Multifunctional superwetting positively charged foams for continuous oil/water emulsion separation and removal of hazardous pollutants from water. Separation and Purification Technology, 2022, 289, 120683.	3.9	19
167	Self-Assembly of Hydrofluorinated Janus Graphene Monolayer: A Versatile Route for Designing Novel Janus Nanoscrolls. Scientific Reports, 2016, 6, 26914.	1.6	18
168	S-graphite slit pore: A superior selective adsorbent for light hydrocarbons. Applied Surface Science, 2018, 444, 772-779.	3.1	18
169	Sixâ€arm Stellat Dendriticâ€PbS Flexible Infrared Photodetector for Intelligent Healthcare Monitoring. Advanced Materials Technologies, 2022, 7, .	3.0	18
170	Theoretical study of H 2 separation performance of two-dimensional graphitic carbon oxide membrane. International Journal of Hydrogen Energy, 2017, 42, 13120-13126.	3.8	17
171	Improving the performance of lithium ion capacitor by stabilizing anode working potential using CoSe2 nanoparticles embedded nitrogen-doped hard carbon microspheres. Electrochimica Acta, 2021, 370, 137717.	2.6	17
172	Anomalous current–voltage characteristics and colossal electroresistance of amorphous carbon film on Si substrate. Applied Physics Letters, 2004, 85, 4397.	1.5	16
173	High-performance aqueous sodium-ion battery using a hybrid electrolyte with a wide electrochemical stability window. RSC Advances, 2020, 10, 25496-25499.	1.7	16
174	End Group Modification for Black Phosphorus: Simultaneous Improvement of Chemical Stability and Gas Sensing Performance. ACS Applied Materials & Interfaces, 2021, 13, 50270-50280.	4.0	16
175	Great enhancement in H2 response using graphene-based Schottky junction. Materials Letters, 2014, 135, 151-153.	1.3	15
176	Molecular Simulation of Oil Mixture Adsorption Character in Shale System. Journal of Nanoscience and Nanotechnology, 2017, 17, 6198-6209.	0.9	15
177	A ZIF-8@H:ZnO core–shell nanorod arrays/Si heterojunction self-powered photodetector with ultrahigh performance. Journal of Materials Chemistry C, 2019, 7, 5172-5183.	2.7	15
178	Amorphous Se species anchored into enclosed carbon skeleton bridged by chemical bonding toward advanced K-Se batteries. Journal of Energy Chemistry, 2021, 61, 319-326.	7.1	15
179	Effect of functional groups on the radial collapse and elasticity of carbon nanotubes under hydrostatic pressure. Nanoscale, 2012, 4, 3894.	2.8	14
180	Enhanced photovoltaic characteristics of MoS ₂ /Si hybrid solar cells by metal Pd chemical doping. RSC Advances, 2016, 6, 1346-1350.	1.7	14

#	Article	IF	CITATIONS
181	Numerical simulation of enhancing shale gas recovery using electrical resistance heating method. International Journal of Heat and Mass Transfer, 2019, 128, 1218-1228.	2.5	14
182	Autonomous Drug Release Systems with Disease Symptomâ€Associated Triggers. Advanced Intelligent Systems, 2020, 2, 1900124.	3.3	14
183	Forward tunneling effect and metal-insulator transition in the BaTiO3 film/Si n-n heterojunction. Applied Physics Letters, 2007, 91, 212105.	1.5	13
184	Molecule Delivery by the Domino Effect of Carbon Nanotubes. Journal of Physical Chemistry C, 2011, 115, 20471-20480.	1.5	13
185	Surface lattice reconstruction enhanced the photoresponse performance of a self-powered ZnO nanorod arrays/Si heterojunction photodetector. Journal of Materials Chemistry C, 2020, 8, 17440-17449.	2.7	13
186	Ni-doped brochantite@copper hydroxide hierarchical structures on copper mesh with ultrahigh oil-resistance for high-efficiency oil/water separation. Surface and Coatings Technology, 2021, 406, 126642.	2.2	13
187	Investigation of the interactions between molecules of β-Carotene, Vitamin A and CNTs by MD simulations. Materials Letters, 2009, 63, 319-321.	1.3	12
188	Carbon nanoscroll from C ₄ H/C ₄ F-type graphene superlattice: MD and MM simulation insights. Physical Chemistry Chemical Physics, 2015, 17, 3441-3450.	1.3	12
189	Defective germanene as a high-efficiency helium separation membrane: a first-principles study. Nanotechnology, 2017, 28, 135703.	1.3	12
190	Mixed Matrix Membranes with Excellent CO ₂ Capture Induced by Nanoâ€Carbon Hybrids. ChemNanoMat, 2017, 3, 560-568.	1.5	12
191	Fluorine-rich carbon nanoscrolls for CO2/CO (C2H2) adsorptive separation. Journal of CO2 Utilization, 2017, 21, 429-435.	3.3	12
192	The effect of oxygen molecule on the hydrogen storage process of Li-doped graphene. Chemical Physics Letters, 2014, 599, 100-103.	1.2	11
193	Effect of interfacial layer on water flow in nanochannels: Lattice Boltzmann simulations. Physica B: Condensed Matter, 2016, 487, 18-24.	1.3	11
194	Trace nitrogen-incorporation stimulates dual active sites of nickel catalysts for efficient hydrogen oxidation electrocatalysis. Chemical Engineering Journal, 2022, 445, 136700.	6.6	11
195	Large photoconductivity of Pd doped amorphous carbon film/SiO2/Si. Diamond and Related Materials, 2012, 21, 24-27.	1.8	10
196	Effective Enhancement of Humidity Sensing Characteristics of Novel Thermally Treated MWCNTs/Polyvinylpyrrolidone Film Caused by Interfacial Effect. Advanced Materials Interfaces, 2016, 3, 1600153.	1.9	10
197	Great Enhancement of Selfâ€Powered Photoresponse Performance of C ₃ H ₈ NSiâ€TiO ₂ NRAs/nâ€5i Heterojunction by Buildâ€In and Buildâ€Out Electric Field Jointly Promoting Carrier Separation. Advanced Electronic Materials, 2020, 6, 2000501.	2.6	10
198	Effect of Si substrate on ethanol gas sensing properties of ZnO films. Thin Solid Films, 2011, 519, 6151-6154.	0.8	9

#	Article	IF	CITATIONS
199	Ultrahigh permittivity of polymer nanocomposites based on surface-modified amorphous carbon/MWCNTs shell/core structured nanohybrids. Composites Part A: Applied Science and Manufacturing, 2017, 100, 324-332.	3.8	9
200	Plate-barrier architecture of rGO-TiO2 derived from MXene for constructing well-aligned polymer nanocomposites with excellent dielectric performance. Composites Science and Technology, 2022, 218, 109191.	3.8	9
201	Robust modified nylon mesh for the separation of crude-oil/water emulsion based on the coupling of squeezing coalescence demulsification and sieving separation. Separation and Purification Technology, 2022, 295, 121319.	3.9	9
202	Study on dielectric properties of oil/water random composites. Journal of Electrostatics, 2001, 50, 169-175.	1.0	8
203	Electric Field Manipulated CO ₂ Capture and Sequestration of Calcium-Graphene. Science of Advanced Materials, 2015, 7, 239-248.	0.1	8
204	A tin oxide/silicon heterojunction with a nano litchi shell structure for ultrafast, high-detectivity, self-powered broadband photodetectors. Journal of Materials Chemistry C, 2022, 10, 2049-2059.	2.7	8
205	The effect of gas injection velocity and pore morphology on displacement mechanisms in porous media based on CFD approach. Journal of Natural Gas Science and Engineering, 2022, 101, 104558.	2.1	8
206	A NOVEL MODEL OF DIELECTRIC CONSTANT OF TWO-PHASE COMPOSITES WITH INTERFACIAL SHELLS. International Journal of Modern Physics B, 2002, 16, 3855-3863.	1.0	7
207	Giant magnetoresistance effect in Co–C bulk composites. Journal of Magnetism and Magnetic Materials, 2002, 246, 379-381.	1.0	7
208	Abnormal current–voltage characteristics and metal–insulator transition of amorphous carbon film/silicon heterojunction. Physics Letters, Section A: General, Atomic and Solid State Physics, 2007, 371, 318-321.	0.9	7
209	Mechanical Properties of Hydrogenated Carbon Nanotubes (C ₄ HNTs): A Theoretical Study. Journal of Physical Chemistry C, 2014, 118, 16087-16094.	1.5	7
210	Ultraâ€high dielectric constant of poly(vinylidene fluoride) composites filled with hydroxyl modified graphite powders. Polymer Composites, 2016, 37, 327-333.	2.3	7
211	Functionalization of petroleum coke-based mesoporous carbon for synergistically enhanced capacitive performance. Journal of Materials Research, 2017, 32, 1248-1257.	1.2	7
212	Theoretical study of strain-controlled C2X (XÂ=ÂN, O) membrane for CO2/C2H2 separation. Applied Surface Science, 2020, 530, 147250.	3.1	7
213	Sensing mechanism of acetone adsorption on charged ZnO and ZnSe surfaces: Insights from DFT calculations. Materials Today Communications, 2022, 31, 103238.	0.9	7
214	Preparation of large diameter and low density ZnS microtube arrays via a sacrificial template method. Materials Letters, 2014, 115, 140-143.	1.3	6
215	Studies in the capacitance properties of diaminoalkane-intercalated graphene. Electrochimica Acta, 2014, 148, 220-227.	2.6	6
216	Extracting the inner wall from nested double-walled carbon nanotube by platinum nanowire: molecular dynamics simulations. RSC Advances, 2017, 7, 39480-39489.	1.7	6

#	Article	IF	CITATIONS
217	Helical wrapping of long-chained polyacetylene (PA) on metallic nanowires: MD simulation insights. Computational Materials Science, 2016, 117, 103-109.	1.4	5
218	Confined hetero double helix structure induced by graphene nanoribbon. 2D Materials, 2019, 6, 034001.	2.0	5
219	Dual carbon Li-ion capacitor with high energy density and ultralong cycling life at a wide voltage window. Science China Materials, 2022, 65, 2373-2384.	3.5	5
220	Study of giant magnetoresistance and giant electroresistance of carbon based thin film. Rare Metals, 2006, 25, 617-620.	3.6	4
221	Controlled growth of hierarchical ZnO nanorods with periodical structure under negative feedback mechanism. Journal Physics D: Applied Physics, 2008, 41, 195402.	1.3	4
222	Influence of polarity on filling polymer molecules into carbon nanotubes. Computational Materials Science, 2011, 50, 2909-2917.	1.4	4
223	Influence of interfaces on impedance response and breakdown of oxide–metal multilayer structures. Thin Solid Films, 2011, 519, 3196-3202.	0.8	4
224	Carbon/Silicon Heterojunction Formed by Inserting Carbon Nanotubes into Silicon Nanotubes: Molecular Dynamics Simulations. Journal of Physical Chemistry C, 2012, 116, 23181-23187.	1.5	4
225	Influence of substrate resistivity on photovoltaic characteristics of Pdâ€doped amorphous carbon film/SiO ₂ /Si heterojunction. Physica Status Solidi (A) Applications and Materials Science, 2012, 209, 1359-1362.	0.8	4
226	High performance sponge MnO ₂ nanotube monoliths. RSC Advances, 2015, 5, 60831-60834.	1.7	4
227	TiO ₂ @TiO _{2â^'x} Hx core-shell nanoparticle film/Si heterojunction for ultrahigh detectivity and sensitivity broadband photodetector. Nanotechnology, 2019, 30, 415203.	1.3	4
228	Folding 2D Graphene Nanoribbons into 3D Nanocages Induced by Platinum Nanoclusters. Journal of Physical Chemistry C, 2020, 124, 10495-10501.	1.5	4
229	Review—Open-Framework Structure Based Cathode Materials Coupled with Metallic Anodes for Rechargeable Multivalent Ion Batteries. Journal of the Electrochemical Society, 2020, 167, 160530.	1.3	4
230	Fabrication of carbon nanotube/graphene core/shell nanostructures on SiO2 substrates using organic solvents: A molecular dynamics study. Science Bulletin, 2012, 57, 3030-3035.	1.7	2
231	CH4 and CO2 Adsorption Mechanism in Kaolinite Slit Nanopores as Studied by the Grand Canonical Monte Carlo Method. Journal of Nanoscience and Nanotechnology, 2021, 21, 108-119.	0.9	2
232	Photoelectrochemical Properties of Alkali Metal Doped TiO ₂ Nano-Honeycomb Film. Energy and Environment Focus, 2015, 4, 191-195.	0.3	2
233	The miscible behaviors of C3H8/C8H18(C7H17N) system in nanoslits: Effects of pore size and rock surface wettability. Chemical Engineering Journal, 2022, 431, 133988.	6.6	2
234	Hierarchical NiO Nanoflake Arrays on Nickel Foam as a Supercapacitor Electrode with High Capacitance and High Rate Capability. Journal of Nanoscience and Nanotechnology, 2016, 16, 4169-4173.	0.9	1

#	Article	IF	CITATIONS
235	Effect of the Wettability on Two-Phase Flow Inside Porous Medium at Nanoscale: Lattice Boltzmann Simulations. Journal of Nanoscience and Nanotechnology, 2017, 17, 6620-6625.	0.9	1
236	Quantitative Characterization of the Effect of Interfacial Fluid Layer on Water Flow Inside Nano-Porous Medium Using the Lattice Boltzmann Method. Journal of Nanoscience and Nanotechnology, 2017, 17, 6216-6223.	0.9	1
237	Abnormal current–voltage characteristics and metal–insulator transition of amorphous Fe-doped carbon films on Si substrates. Physica B: Condensed Matter, 2008, 403, 3434-3438.	1.3	0
238	Lattice Boltzmann method for simulation of shale gas flow in kerogen nano-pores considering temperature dependent adsorption. International Journal of Oil, Gas and Coal Technology, 2020, 23, 409.	0.1	0
239	DFT insights into the selective NH ₃ sensing mechanism of two dimensional ZnTe monolayer. Journal of Physics Condensed Matter, 2022, 34, 374002.	0.7	0